A mechanism for regional variations in snowpack melt under rising temperature

Amato Evan [ID] [✉] and Ian Eisenman [ID]

As the planet warms, mountain snowpack is expected to melt progressively earlier each spring. However, analysis of measurements in the western United States shows that the change in the date when snowpack disappears is not uniform: for 1°C of warming, snowpack disappears 30 days earlier in some regions, whereas there is almost no change in others. Here we present an idealized physical model that simulates the timing of snowpack melt under changing temperature and use it to show that this observed disparity in the sensitivity of snowpack disappearance to warming results from a mechanism related to the sinusoidal shape of the annual cycle of temperature. Applying this model globally, we show that under uniform warming the timing of snowpack disappearance will change most rapidly in coastal regions, the Arctic, the western United States, Central Europe and South America, with much smaller changes in the northern interiors of North America and Eurasia.

There is a large body of work examining the effect of rising temperatures on snow in the western United States (hereafter the west). Long-term measurements of mountain stream-flow[1,2] and 1 April snow water equivalent[3,4] (hereafter referred to as snowpack) suggest that over time the mass of snow in the mountains of the west is in decline. In the west, the freshwater supply is dependent upon meltwater from mountain snow and storage of that water in reservoirs[5]. Model simulations show that with precipitation held constant, springtime melting of mountain snowpack will occur progressively earlier in the water year as air temperatures increase[6–8], with potentially adverse effects on the freshwater supply of the west, primarily due to early season flooding, exceedance of reservoir capacity and a lack of runoff late in the season[9,10]. In addition, early season snowmelt can lengthen the duration of the dry season in some parts of the west, with implications for wildfire risk[11,12]. However, in the recent observational record there are not widespread and statistically significant downward trends in snow-melt timing across the West[13,14], although this may be expected given that such trends are strongly influenced by year-to-year changes in precipitation[15,16].

Given observed past and potential future changes in mountain snowpack, quantifying and understanding the influence of increasing temperatures is of interest. Here we focus on changes in the water-year date when snow completely melts, as this date is a natural metric for signifying the end of the winter season. To do so, we utilize 37 years (1982–2018 water years) of daily snow water equivalent, S, measurements from 398 sites managed by the Natural Resources Conservation Service Snowpack Telemetry (SNOTEL) network[14,17] (description in Methods). We define the snowpack disappearance date, ζ, for each station as the water-year day when $S = 0$ following the seasonal peak in S (Fig. 1), where the water year begins on 1 October and is defined as the year of the following spring season. We estimate daily mean surface air temperature, T, and precipitation, P, over these same years for each of these stations via interpolation of temperature and precipitation fields from the North American Regional Reanalysis[18] (NARR; Methods). All SNOTEL locations used in this study are shown in Fig. 2.
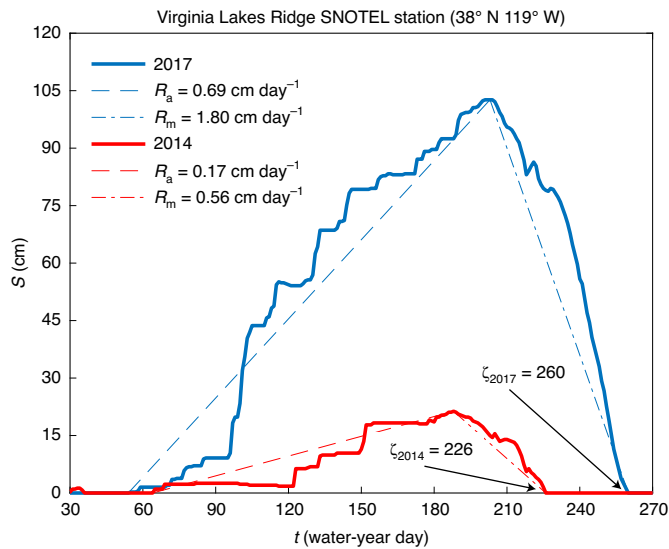
Both precipitation and temperature influence ζ[8]. For example, Fig. 1 shows daily time series of S measured by a SNOTEL station in the Sierra Nevada mountain range for the 2014 and 2017 water years. During 2014 S peaks at 21 cm, while in 2017 S is larger by nearly a factor of five (103 cm). Consistent with this, the snowpack melt date ζ is more than 30 days later in the season in 2017: $\zeta = 226$ in 2014 and $\zeta = 260$ in 2017. The change in S and ζ between these two years was driven by both precipitation and temperature; the annual mean precipitation in 2017 was three-fold greater and the annual mean temperature was 1°C cooler than in 2014. As such, we estimate the sensitivity of the snowpack disappearance date to temperature using a multilinear regression of ζ onto water-year mean temperature T_0 and precipitation P_0, that is:

$$\mathrm{d}\zeta = \frac{\partial \zeta}{\partial T_0}\delta T_0 + \frac{\partial \zeta}{\partial P_0}\delta P_0,$$

with $\partial\zeta/\partial T_0$ the resulting sensitivity of snowpack disappearance date to temperature for constant precipitation (Methods).

A map of $\partial\zeta/\partial T_0$ calculated from SNOTEL measurements of S and NARR T and P shows spatial heterogeneity in the sensitivity of the date when snowpack disappears to temperature (Fig. 2a). Some of the largest magnitude values are found in the Pacific Northwest (125–120° W and 43–48° N) and the southwest (south of 35° N), where $\partial\zeta/\partial T_0$ can be lower than −30 days °C⁻¹. In contrast, in the interior of the continent $\partial\zeta/\partial T_0$ is far smaller in magnitude, with values in the Southern Rocky Mountains near −5 days °C⁻¹, and close to zero in the mountain ranges of northern Utah. The results in Fig. 2a are consistent with those from a previous analysis of SNOTEL data, which had implied a sensitivity of snowpack duration, the amount of time the surface is covered with snow during a water year, to mean temperature[8]. These results are also similar to previous work finding that downward trends in 1 April S are largest in the warmest regions of the West[19].

To investigate the source of the heterogeneity in the spatial structure of $\partial\zeta/\partial T_0$, we develop a highly idealized model of snowpack accumulation and ablation that is a function of daily mean surface air temperature, T (Methods), which we approximate to vary sinusoidally over the course of the year as

Scripps Institution of Oceanography, University of California, San Diego, La Jolla, CA, USA. ✉e-mail: aevan@ucsd.edu

Fig. 1 | Examples of observed snowpack for two water years. Plotted are measurements of S from the Virginia Lakes Ridge SNOTEL station in California for the 2014 (red solid line) and 2017 (blue solid line) water years. The value of ζ, which is defined as the first water-year day when $S = 0$ following the seasonal peak in S, is indicated for each year. The lines indicating the seasonal-average rate of accumulation, R_a (dashed line), and melt, R_m (dash-dotted line), are also plotted for each year.

$$T = T_0 - T_1 \sin(\omega t - \phi) \tag{1}$$

where T_1 is the amplitude of the annual cycle, t is time, ϕ is a phase shift in time and ω is $2\pi/365$ days^{-1} (Supplementary Fig. 1a). We treat precipitation as a constant from the beginning of the water year $t = 0$ until a specified later time $t = t_p$, after which there is zero precipitation (Supplementary Fig. 1c).

Next, snowpack may melt when the skin temperature is 0 °C but the corresponding temperature of the overlying air may be greater than or less than this value. To account for differences between the skin and air temperature at the melting point, in our model snowpack melts at the constant rate R_m when $T > T_m$, where T_m is the surface air temperature at which snowmelt occurs, which may be greater than, less than or equal to 0 °C. For simplicity, snowpack accumulates at the constant rate R_a when $T < T_m$, which is a limitation of our approach as the air temperatures corresponding to melting and accumulation at the surface are not constrained to be identical in the real world. Both R_a and R_m (given in cm day^{-1}) are positive and do not depend on the magnitude of the departures of T from T_m (Supplementary Fig. 1c). We analytically solve this model for ζ and then take the partial derivative with respect to T_0 (Methods) to obtain

$$\frac{\partial \zeta}{\partial T_0} = -\frac{1}{\omega} \frac{1}{\sqrt{T_1^2 - (T_0 - T_m)^2}} \left(1 + \frac{R_a}{R_m}\right). \tag{2}$$

From equation (2), the sensitivity $\partial\zeta/\partial T_0$ is always negative since warming leads to earlier melt. The magnitude of $\partial\zeta/\partial T_0$ is large when the difference between T_1 and $|T_0 - T_m|$ is small, in which case the temperature either spends most of the year above the melting point or most of the year below the melting point. Equation (2) is undefined if $T_1 < |T_0 - T_m|$ since this would imply that the annual cycle does not include temperatures both below and above the melting point.

The mechanism behind the dependence of $\partial\zeta/\partial T_0$ on T_0, T_m and T_1 in equation (2) is related to the shape of the seasonal cycle in T. Assuming for simplicity of explanation that $T_m = 0$ °C, in regions where $T_0 > 0$ and T_1 is only slightly larger than $|T_0|$, T crosses zero near the flat trough of the sinusoid, with temperatures below zero occurring only during a brief part of the year. In this case, when T warms there is a large reduction in the number of days when $T < 0$, leading to a substantially earlier time of complete snowmelt. A similar argument applies in regions where $T_0 < 0$ and T_1 is only slightly larger than $|T_0|$, in which case T rises above the melting point near the flat crest of the sinusoid and a small warming also leads to a large reduction in the duration with $T < 0$. Hence the magnitude of $\partial\zeta/\partial T_0$ is larger where T_1 is more similar to $|T_0|$, that is, where the annual minimum or maximum temperature is near the melting point. A schematic of the influence of T_0 and T_1 on $\partial\zeta/\partial T_0$ can be found in Extended Data Fig. 1.

We estimate R_a and R_m from SNOTEL measurements of S, where R_a is the annual maximum value of S divided by the length of time t that S is increasing, and R_m is the annual maximum value of S divided by the length of time that S is decreasing (for example, Fig. 1). The ratio R_a/R_m is fairly constant in the data. For example, the value of this ratio differs by less than 25% between the vastly different 2014 and 2017 water years at the Virginia Lakes SNOTEL station (Fig. 1). The average of the SNOTEL stations' long-term mean values of this ratio is 0.34 ± 0.14. We estimate T_m for each SNOTEL site as the coolest daily mean temperatures for which the one-day change in S is negative, using the long-term mean (1982–2018) seasonal cycles of T and S. The SNOTEL-station-averaged T_m is 0.18 ± 2.02 °C.

A map of the values of $\partial\zeta/\partial T_0$ predicted by equation (2) is shown in Fig. 2b, based on the long-term mean values of T_1, T_0 and R_a/R_m at each SNOTEL station and the station-averaged value of T_m. The idealized model reproduces the spatial structure of the observations (Fig. 2a), with the largest magnitude values in coastal and southern regions and the smallest magnitudes towards the interior. The correlation between equation (2) and observations is positive and statistically significant (r value = 0.77, P value < 0.01), and the bias and root mean squared error (RMSE) are −0.3 and 3.9 days °C^{-1}, respectively, relative to a mean value of $d\zeta/dT_0$ of −10.5 days °C^{-1}.

According to equation (2), and again assuming for simplicity of explanation that $T_m = 0$ °C, in the west the largest magnitudes of $\partial\zeta/\partial T_0$ occur in locations where the difference between T_1 and T_0 is small (Fig. 2). Thus, the largest magnitudes of $\partial\zeta/\partial T_0$ are found in the Pacific Northwest and California, where annual mean T is large but the annual cycle of T is small, and thus $|T_1 - T_0|$ is also small (approximately < 5 °C). Conversely, the smallest magnitude values of $\partial\zeta/\partial T_0$ are found far from the coast, where annual mean T is closer to zero but the magnitude of the annual cycle of T is large, such that $|T_1 - T_0|$ is larger (between approximately 5 and 11 °C). The high-magnitude values of $\partial\zeta/\partial T_0$ found south of 35° N result from both a large annual mean T and a large seasonal cycle amplitude of T.

A direct comparison of $\partial\zeta/\partial T_0$ calculated from the SNOTEL and NARR data and from equation (2) shows some disagreement in the two estimates, particularly at large magnitudes (Fig. 3a). Some of this scatter is probably due to uncertainty in the multilinear regression; the vertical error bars represent the 95% uncertainty level in the regression used to calculate $\partial\zeta/\partial T_0$, 89% of which spans the equivalency line between the two estimates (black dashed). The slope of a linear least-squares regression line for these data is 1.0 ± 0.1, suggesting that the disagreement is not dependent on the magnitude of $\partial\zeta/\partial T_0$.

Continuous daily measurements of T and P are available for 363 of the SNOTEL stations used here for the 2001–2018 water years, and so we repeated the above analysis using only measurements. For each station, we estimated the long-term mean T_0, T_1, ϕ and
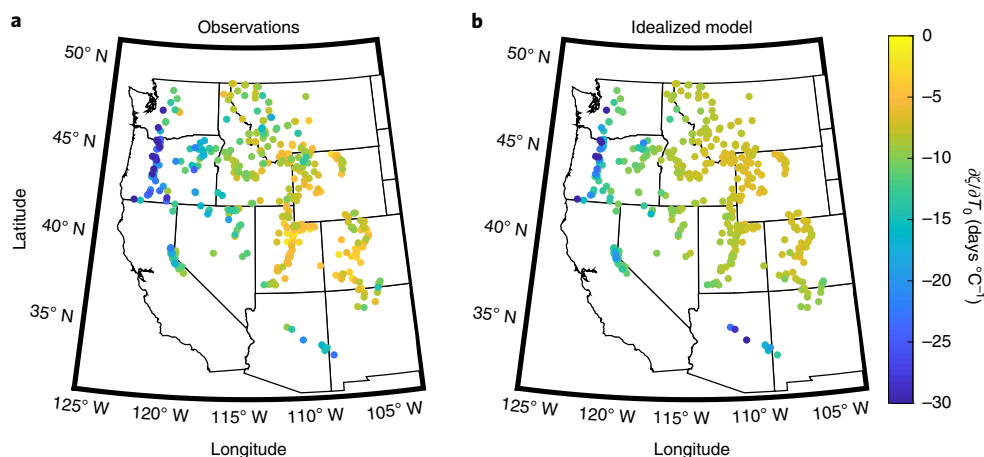
Fig. 2 | Maps of the sensitivity of the timing of snowpack date of disappearance to temperature. a, The observed change in the day of complete snowpack melt per degree of warming ($\partial\zeta/\partial T_0$), which is calculated from daily measurements of snowpack (S), at each of the 398 SNOTEL stations used in the analysis over the 1982–2018 water years. **b,** The prediction for $\partial\zeta/\partial T_0$ based on the idealized model (equation (2)).

T_m from daily measurements of T and then used these values to determine $\partial\zeta/\partial T_0$ from multilinear regression and equation (2). The results are similar to those shown in Fig. 3a; the correlation in $\partial\zeta/\partial T_0$ calculated from observations and via equation (2) is positive and statistically significant (r value = 0.64, P value < 0.01), and the bias and RMSE in equation (2) are 1.1 and 5.8 days °C^{-1}, respectively (Supplementary Fig. 2a).

In the real world, mountain snowpack is shaped by a large number of complex surface processes[20,21] that are overly simplified or not accounted for in the idealized model. Thus, to better understand the utility and limitations of the idealized model, we carried out a set of simulations with the Variable Infiltration Capacity (VIC) hydrologic model[22,23], a land-surface model that simulates a comprehensive array of physical processes governing snowpack state. We forced the VIC model with long-term mean NARR output interpolated to the SNOTEL stations, but altered the annual cycle of daily mean temperature to follow equation (1) (VIC simulation details in Methods), where T_0 and T_1 were taken from observations. For each station, we conducted a set of simulations so that T_0 spanned ±0.5 °C. We then calculated $\partial\zeta/\partial T_0$ directly from the VIC output and via equation (2), where R_a, R_m and T_m were calculated from the VIC output.

The agreement between the two estimates of $\partial\zeta/\partial T_0$ for the VIC model is nearly exact (Fig. 3b); the two are correlated with an r value of 0.97 (P value < 0.01). Thus, the idealized model (equation (2)) can effectively explain all of the variance in $\partial\zeta/\partial T_0$ in a model that represents the complex physical processes governing the annual cycle of snowpack. We note that the range of $\partial\zeta/\partial T_0$ from the VIC output does not match that from SNOTEL (Fig. 3a); because T_m and R_a/R_m from the VIC model are larger and smaller, respectively, than those values calculated from SNOTEL/NARR measurements, the VIC-averaged T_m is 1.03 ± 0.45 and R_a/R_m is 0.28 ± 0.05.

To explore the disagreement in estimates of $\partial\zeta/\partial T_0$ from equation (2) (Fig. 3a) we conducted additional VIC simulations using the actual NARR T, rather than forcing T to exactly follow a sinusoid (Methods). In this case, $\partial\zeta/\partial T_0$ calculated from equation (2) underestimates that calculated directly from the VIC model output via linear regression (Supplementary Fig. 3). An analysis of the differences between reanalysis T and T from equation (1) suggests that this is because T increases more rapidly from the wintertime minimum than does a perfect sinusoid. Thus, the idealized model begins to break down as T deviates from a sinusoid, tending to underestimate the true magnitude of $\partial\zeta/\partial T_0$.

Based on the analysis of SNOTEL measurements of S and NARR T and P (Figs. 2 and 3a), SNOTEL measured S, T and P (Supplementary Fig. 2), and output from the VIC model (Fig. 3b), the idealized model provides a robust and straightforward method to understand how increasing temperatures affect the date of snowpack disappearance, ζ. Therefore, we next extend the idealized model to examine changes in ζ outside the west. According to equation (2), $\partial\zeta/\partial T_0$ is symmetric about $T_0 - T_m = 0$ (Supplementary Fig. 4). The symmetry suggests that large magnitudes of $\partial\zeta/\partial T_0$ should also occur in cold regions (that is, $T_0 < T_m$) where the amplitude of the annual cycle of T is relatively small, such that $T_1 + (T_0 - T_m)$ is close to zero (schematic in Extended Data Fig. 1). We attempted to test for this symmetry via analysis of continuous measurements of T and P made at 14 SNOTEL stations in Alaska during the 2008–2018 water years. For these 14 stations, the correlation in $\partial\zeta/\partial T_0$ calculated from equation (2) and linear regression was positive and statistically significant (r value = 0.76, P value < 0.01; Supplementary Fig. 2b). However, although T_0 for these stations was near 0 °C, T_1 was large, ranging from 9 °C to 19 °C. Nonetheless, these results suggest that the idealized model has validity at high latitudes.

We apply the idealized model globally by calculating $\partial\zeta/\partial T_0$ via equation (2) using long-term (1982–2018) mean seasonal cycles of T_0 and T_1 estimated from a global reanalysis[24], and assuming R_a/R_m and T_m to be the mean values calculated over the west, 0.34 and 0.18 °C, respectively. Based on the calculations with equation (2), within the Northern Hemisphere the magnitude of $\partial\zeta/\partial T_0$ is largest along the coasts (including in polar regions), throughout the west, across North America near 40° N latitude and within Central Europe (Fig. 4a). Within the interior of northern North America and Eurasia, however, $\partial\zeta/\partial T_0$ has smaller magnitudes, between −6 and −3 days °C^{-1}.

Adopting here again for simplicity of discussion that $T_m = 0$ °C, from an analysis of these global estimates of $\partial\zeta/\partial T_0$ (Fig. 4a), large magnitude values of $\partial\zeta/\partial T_0$ are found in locations where T_1 is small and $|T_0|$ is large (that is, high- and low-latitude coastal regions) or where T_0 and T_1 are both large (that is, inland and at lower latitudes), which can be seen in a parameter-space diagram of these global values of $\partial\zeta/\partial T_0$ (Supplementary Fig. 5). For example, the magnitude of $\partial\zeta/\partial T_0$ is large along the Greenland coast and poleward of 75° N, where T_0 is negative and the same order of magnitude as T_1 (schematic in Extended Data Fig. 1). Large magnitude values are also seen in many coastal regions at lower latitudes, such as the western coasts of North America and Europe, where T_1 is small and
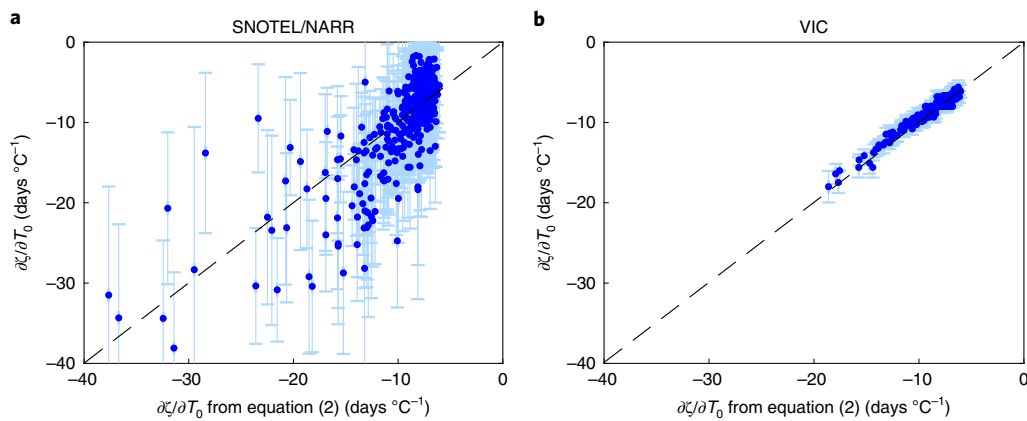
Fig. 3 | Comparisons of $\partial\zeta/\partial T_0$ calculated from SNOTEL observations and reanalysis and from the VIC model. a,b, Plotted on the vertical axis are values of $\partial\zeta/\partial T_0$ calculated for individual SNOTEL stations from observations and reanalysis (**a**) and the output of the VIC model (**b**) via linear regression, and on the horizontal axis $\partial\zeta/\partial T_0$ calculated from the idealized model (equation (2)). The vertical error bars represent the 95% uncertainty in the regression coefficient used to determine $\partial\zeta/\partial T_0$. The black dashed lines represent equivalence between the two calculated values of $\partial\zeta/\partial T_0$.
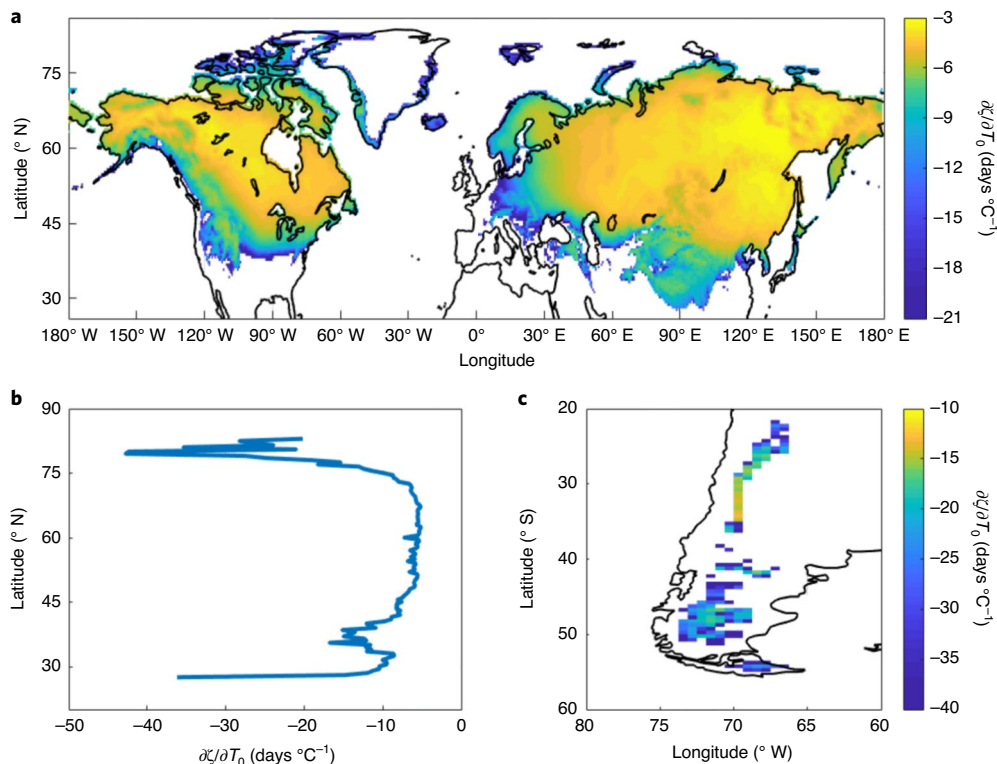
Fig. 4 | Global estimates of $\partial\zeta/\partial T_0$. a, $\partial\zeta/\partial T_0$ calculated via equation (2), where T_0 and T_1 are estimated from a global reanalysis[24] with $R_a/R_m = 0.34$ and $T_m = 0.18$. White shading represents regions where $\partial\zeta/\partial T_0$ is undefined (over water, or where $T_1 < |T_0 - T_m|$). **b,** The same values of $\partial\zeta/\partial T_0$ as in **a**, but averaged over all longitudes and plotted as a function of latitude in the northern hemisphere (vertical axis). **c,** Values of $\partial\zeta/\partial T_0$ over southern South America. Note that to increase the contrast in these plots, the colour bars in **a** and **c** are not identical, and these scales are both different from that in Fig. 2.

T_0 is positive, similar to the case of the Pacific Northwest in Fig. 2a. At lower latitudes, the magnitude of $\partial\zeta/\partial T_0$ is large near the southern boundary of where $\partial\zeta/\partial T_0$ is defined (south of 45° N in North America and Asia, and in Central Europe), where T_1 is large but T_0 is also large and positive. Values of $\partial\zeta/\partial T_0$ within continental interiors are closer to 0 days °C^{-1} because in these regions T_0 is close to 0 °C and T_1 is large. This explains why, when averaged over longitude, in the Northern Hemisphere the magnitude of $\partial\zeta/\partial T_0$ is largest south of 30° N, where $T_0 > 0$ °C, and poleward of 75° N, where $T_0 < 0$ °C

(Fig. 4b). In the Southern Hemisphere, $\partial\zeta/\partial T_0$ is undefined over most landmasses as $T > 0$ °C the entire year (for example, southern Africa and Australia) or $T < 0$ °C the entire year (for example, Antarctica). Although, in southern South America, the magnitude of $\partial\zeta/\partial T_0$ is less than -30 days °C^{-1} throughout much of the interior of the continent (Fig. 4c).

The maps in Fig. 4 are only valid to the extent that the physical world is similar to that assumed by the idealized model. To test this, we again ran the VIC model poleward of 60° N, but this

time forced with the global reanalysis (Methods). We then calculated $\partial\zeta/\partial T_0$ directly from the model output and via equation (2). We found a positive correlation between $\partial\zeta/\partial T_0$ calculated from the VIC model via linear regression and $\partial\zeta/\partial T_0$ calculated from the idealized model via equation (2) (r value = 0.62, P value < 0.01; Supplementary Fig. 6), suggesting that the idealized model may be capturing the true spatial pattern of $\partial\zeta/\partial T_0$. However, the idealized model also underestimates the magnitude of $\partial\zeta/\partial T_0$ at large magnitudes of $\partial\zeta/\partial T_0$, and thus the actual values of $\partial\zeta/\partial T_0$ may be more negative than those shown in Fig. 4. The similarity in the structure of the biases in Supplementary Figs. 3 and 6 suggests that the source of the bias may be departures of reanalysis T from a sinusoid. We explored validation of the results in Fig. 4 using satellite-based estimates of snow cover. However, we found that the available data were too coarsely resolved in time (for example, weekly resolution) or too short in duration (for example, only 15 years in length), such that the estimates of $\partial\zeta/\partial T_0$ were unlikely to be significantly different from zero.

A substantial fraction of the global population relies on river water from snowpack melt for potable water, and shifts in the timing of that melt affect the availability of this crucial resource[10]. Changes in ζ result from changes in the timing of the onset of snow ablation[14,25]. As such, these results suggest that water resources may be most stressed in regions that rely heavily on snowpack from coastal and low-latitude mountains, including Western and Central Europe. Lastly, the Arctic is projected to warm more rapidly than anywhere else on the planet[26,27]. The idealized model presented here suggests that the Arctic is also the region with the greatest sensitivity of the springtime snowpack to warming (Fig. 4b). Taken together, these results suggest that the Arctic may undergo a dramatically rapid shift in the date when snowpack completely melts under future warming.

Online content

Any methods, additional references, Nature Research reporting summaries, source data, extended data, supplementary information, acknowledgements, peer review information; details of author contributions and competing interests; and statements of data and code availability are available at https://doi.org/10.1038/s41558-021-00996-w.

References

1. Cayan, D. R., Kammerdiener, S. A., Dettinger, M. D., Caprio, J. M. & Peterson, D. H. Changes in the onset of spring in the western United States. *Bull. Am. Meteorol. Soc.* **82**, 399–416 (2001).
2. Stewart, I. T., Cayan, D. R. & Dettinger, M. D. Changes toward earlier streamflow timing across western North America. *J. Clim.* **18**, 1136–1155 (2005).
3. Mote, P. W. Climate-driven variability and trends in mountain snowpack in western North America. *J. Clim.* **19**, 6209–6220 (2006).
4. Mote, P. W., Li, S., Lettenmaier, D. P., Xiao, M. & Engel, R. Dramatic declines in snowpack in the western US. *NPJ Clim. Atmos. Sci.* **1**, 2 (2018).
5. Doesken, N. & Judson, A. *The Snow Booklet: A Guide to the Science, Climatology, and Measurement of Snow in the United States* (Colorado State Univ., 1996).
6. Lettenmaier, D. P. & Gan, T. Y. Hydrologic sensitivities of the Sacramento–San Joaquin River basin, California, to global warming. *Water Resour. Res.* **26**, 69–86 (1990).
7. Hamlet, A. F., Mote, P. W., Clark, M. P. & Lettenmaier, D. P. Effects of temperature and precipitation variability on snowpack trends in the western United States. *J. Clim.* **18**, 4545–4561 (2005).
8. Luce, C. H., Lopez-Burgos, V. & Holden, Z. Sensitivity of snowpack storage to precipitation and temperature using spatial and temporal analog models. *Water Resour. Res.* **50**, 9447–9462 (2014).
9. Hamlet, A. F. & Lettenmaier, D. P. Effects of climate change on hydrology and water resources in the Columbia River basin. *J. Am. Water Resour. Assoc.* **35**, 1597–1623 (1999).
10. Barnett, T. P., Adam, J. C. & Lettenmaier, D. P. Potential impacts of a warming climate on water availability in snow-dominated regions. *Nature* **438**, 303–309 (2005).
11. Westerling, A. L., Hidalgo, H. G., Cayan, D. R. & Swetnam, T. W. Warming and earlier spring increase western US forest wildfire activity. *Science* **313**, 940–943 (2006).
12. Gergel, D. R., Nijssen, B., Abatzoglou, J. T., Lettenmaier, D. P. & Stumbaugh, M. R. Effects of climate change on snowpack and fire potential in the western USA. *Climatic Change* **141**, 287–299 (2017).
13. Zeng, X., Broxton, P. & Dawson, N. Snowpack change from 1982 to 2016 over conterminous United States. *Geophys. Res. Lett.* **45**, 12940–12947 (2018).
14. Evan, A. T. A new method to characterize changes in the seasonal cycle of snowpack. *J. Appl. Meteorol. Climatol.* **58**, 131–143 (2019).
15. Pierce, D. W. & Cayan, D. R. The uneven response of different snow measures to human-induced climate warming. *J. Clim.* **26**, 4148–4167 (2013).
16. Mankin, J. S. & Diffenbaugh, N. S. Influence of temperature and precipitation variability on near-term snow trends. *Clim. Dyn.* **45**, 1099–1116 (2015).
17. Serreze, M. C., Clark, M. P., Armstrong, R. L., McGinnis, D. A. & Pulwarty, R. S. Characteristics of the western United States snowpack from snowpack telemetry (SNOTEL) data. *Water Resour. Res.* **35**, 2145–2160 (1999).
18. Mesinger, F. et al. North American regional reanalysis. *Bull. Am. Meteorol. Soc.* **87**, 343–360 (2006).
19. Mote, P. W., Hamlet, A. F., Clark, M. P. & Lettenmaier, D. P. Declining mountain snowpack in western North America. *Bull. Am. Meteorol. Soc.* **86**, 39–49 (2005).
20. Anderson, E. A. Development and testing of snow pack energy balance equations. *Water Resour. Res.* **4**, 19–37 (1968).
21. Andreadis, K. M., Storck, P. & Lettenmaier, D. P. Modeling snow accumulation and ablation processes in forested environments. *Water Resour. Res.* **45**, W05429 (2009).
22. Liang, X., Lettenmaier, D. P., Wood, E. F. & Burges, S. J. A simple hydrologically based model of land surface water and energy fluxes for general circulation models. *J. Geophys. Res. Atmos.* **99**, 14415–14428 (1994).
23. Hamman, J. J., Nijssen, B., Bohn, T. J., Gergel, D. R. & Mao, Y. The Variable Infiltration Capacity model version 5 (VIC-5): infrastructure improvements for new applications and reproducibility. *Geosci. Model Dev.* **11**, 3481–3496 (2018).
24. Gelaro, R. et al. The Modern-Era Retrospective Analysis for Research and Applications, version 2 (MERRA-2). *J. Clim.* **30**, 5419–5454 (2017).
25. Trujillo, E. & Molotch, N. P. Snowpack regimes of the western United States. *Water Resour. Res.* **50**, 5611–5623 (2014).
26. Holland, M. M. & Bitz, C. M. Polar amplification of climate change in coupled models. *Clim. Dyn.* **21**, 221–232 (2003).
27. Collins, M. et al. in *Climate Change 2013: The Physical Science Basis* (eds Stocker, T. F. et al.) Ch. 12 (IPCC, Cambridge Univ. Press, 2013).

Methods

Data. The SNOTEL station data used in this study are described in ref. [14]. We considered a station to have continuous measurements of S, T and P if, for a given water year, these data were missing for fewer than 30 days. We interpolated the gridded NARR output for 2 m air temperature, which has a nominal 32 km horizontal resolution, to the locations of the SNOTEL stations used in this analysis (Fig. 2a) via an inverse-distance-weighting method. On average, the weighted elevation of the interpolated NARR data is 250 ± 277 m lower than the elevation of the corresponding SNOTEL station, resulting in a net warm bias in T_0. To account for this difference in height, we obtained a correction factor for each station on the basis of the differences in averaged (2001–2018) T_0 from the interpolated reanalysis and from the SNOTEL measurements. There was also a positive bias in T_1 in the interpolated NARR data, and we corrected these values in an identical manner.

When calculating $\partial\zeta/\partial T_0$ from the multilinear regression we use water-year mean precipitation P_0. We note that nearly identical results are obtained when defining P_0 as precipitation only during the boreal winter and spring seasons or as winter season only. To create global estimates of $\partial\zeta/\partial T_0$ via equation (2), we calculated T_0 and T_1 from the long-term (1982–2018) monthly mean temperatures output from a global reanalysis[24], at a horizontal resolution of 0.5° (Supplementary Fig. 5).

Idealized model. Daily mean temperature T is given by equation (1) and averaged over all SNOTEL stations and the 1982–2018 water years. The RMSE of this sinusoidal approximation to the long-term mean T from reanalysis is 1.4 ± 0.2 °C. Daily measurements of T are available for 268 of these SNOTEL stations during the 1995–2018 water years. We also fit these annual cycles of measured T to equation (1), and here the RMSE of the long-term mean and measured T is also 1.4 °C (Supplementary Fig. 1a,b). Thus, equation (1) is a reasonable approximation to the annual cycle of T from reanalysis and in-situ measurements in such environments.

The representation of T in equation (1) implies that the time, t_d, that T crosses below the temperature when snow accumulates or melts, T_m, is

$$t_d = \frac{1}{\omega}\,\sin^{-1}\left(\frac{T_0 - T_m}{T_1}\right) + \frac{\phi}{\omega},$$

and the time t_u that T crosses back above T_m is

$$t_u = \frac{\pi}{\omega} - \frac{1}{\omega}\,\sin^{-1}\left(\frac{T_0 - T_m}{T_1}\right) + \frac{\phi}{\omega}.$$

Based on the daily mean precipitation and snowpack accumulation and melt, which are described in the main text, the total snowpack accumulation, A_t, during the water year is equal to the accumulation rate times the duration when there is precipitation and $T < T_m$,

$$A_t = R_a\left(t_p - t_d\right) = R_a\left[t_p - \frac{1}{\omega}\,\sin^{-1}\left(\frac{T_0 - T_m}{T_1}\right) - \frac{\phi}{\omega}\right].$$

where we have assumed for simplicity in the model that $t_p < t_u$.

Similarly, the total snowmelt during the water year, M_t, is equal to the melt rate times the duration when there is snowpack and $T > T_m$,

$$M_t = R_m\left(\zeta - t_u\right) = R_m\left[\zeta - \frac{\pi}{\omega} + \frac{1}{\omega}\,\sin^{-1}\left(\frac{T_0 - T_m}{T_1}\right) - \frac{\phi}{\omega}\right].$$

Since the total snow accumulation must equal the total snowmelt, $A_t = M_t$. Solving this for ζ gives

$$\zeta = \left[\frac{\pi + \phi}{\omega} + \frac{R_a}{R_m}\,\left(t_p - \frac{\phi}{\omega}\right)\right] - \frac{1}{\omega}\,\sin^{-1}\left(\frac{T_0 - T_m}{T_1}\right)\,\left(1 + \frac{R_a}{R_m}\right).$$

We obtain equation (2) by differentiating this expression for ζ with respect to T_0, using the identity $\mathrm{d}/\mathrm{d}x\,(\sin^{-1}x) = (1 - x^2)^{-1/2}$.

To illustrate the application of this idealized model, we estimated T via equation (1) (Supplementary Fig. 1a) from daily measurements of T for the 2017 water year at Virginia Lakes SNOTEL station (Supplementary Fig. 1b), where $T_0 = 4.9$ °C, $T_1 = 9.1$ °C and $\phi = 25.8$ days. We assumed that precipitation is constant from the beginning of the water year until t_p, which we estimated to be water-year day 190 (Supplementary Fig. 1c), based loosely on the site measurements of daily mean P (Supplementary Fig. 1d). In the idealized model, snowpack accumulation occurs at the constant rate R_a if $t < t_p$ and $T < T_m$ and melting occurs at the constant rate R_m if $T > T_m$ (Supplementary Fig. 1e). These are compared with the measured values of each (Supplementary Fig. 1f); R_a and R_m for this case are described in the main text, and T_m is estimated to be 3 °C on the basis of a comparison of measured T and S for this site and water year. The resultant annual cycle of S is then $A - M$ (Supplementary Fig. 1g), which is qualitatively similar to the measured value (Supplementary Fig. 1h). We calculate $\zeta = 260.4$ and $\partial\zeta/\partial T_0 = -9.1$ days °C^{-1}. To

facilitate comparison with observations, in Supplementary Fig. 1g S is smoothed with an 11-day-running-mean filter, as is done for the SNOTEL observations (Supplementary Fig. 1h), where $\zeta = 265$ in both figures.

We note that in our idealized model, R_m is not a function of temperature. Although previous work has shown that R_m decreases under warming[14,28], an analysis of SNOTEL data shows that R_a also decreases with rising temperature (not shown), and consequently the ratio R_a/R_m for each site is somewhat constant with changes in temperature. Averaged over all SNOTEL sites, the derivative of R_a/R_m with respect to annual mean T, which was determined via linear regression, is not statistically different from zero (0.04 ± 0.12 °C^{-1}).

VIC model. We forced the VIC model with three-hour temporal resolution output from NARR interpolated to the SNOTEL station locations via inverse-distance weighting. The forcings were interpolated in time to be hourly. The forcing variables include 2 m air temperature, 2 m dewpoint temperature, precipitation rate, 10 m surface wind speeds, surface pressure and surface fluxes of downward longwave and shortwave radiation. We averaged this station-interpolated data over the 1982–2018 water years and then over all stations to create an input dataset of the annual cycle in each variable that is representative of the average conditions at each of the 398 SNOTEL sites. This averaging results in less snow accumulation than the average SNOTEL value, which is expected since the grid-averaged NARR precipitation values are lower than those from SNOTEL measurements by approximately a factor of three. Thus, we scaled the NARR precipitation data by a constant factor of 1.6 such that the annual cycle of S produced by the VIC model in this parameter regime matched the SNOTEL observations averaged over all water years and SNOTEL stations. We assumed 100% evergreen needleleaf forest cover and used three layers in the soil model and a temporal resolution of one hour.

We then performed 398 sets of simulations, corresponding to the long-term mean values of T_0 and T_1 at each SNOTEL station. Here we forced the annual cycle of daily mean temperature, T, to exactly follow equation (1) but retained the sub-daily variability from NARR. We then incrementally decreased and then increased T_0 by 1/8 °C to span a 1 °C change in T_0. For each simulation, we adjusted the downwelling longwave radiation at the surface to be consistent with the forced changes in T and adjusted vapour pressure to maintain a constant relative humidity, following the methods of Musselman et al.[29]. The results from these simulations are shown in Fig. 3b.

In addition, we reran the model assuming (1) constant vapour pressure, (2) a slight adjustment to the treatment of the corresponding change in longwave radiation and (3) constant precipitation. For each case, the results were nearly identical to those presented Fig. 3b.

We performed a second set of simulations with the VIC model identical to that described above except that we did not force the annual cycle of T to follow equation (1) (Supplementary Fig. 3). We interpret the differences between Fig. 3 and Supplementary Fig. 3 to be due to the influence of departures of T from a pure sinusoid.

We also performed a third set of simulations, this time forcing the model with hourly output from a global reanalysis for the year 2000 and poleward of 60° N[24], where no adjustments to the reanalysis temperature were conducted. We again increased and decreased T in the forcing to span a 1 °C change in T_0 and used the model output and equation (2) to calculate $\partial\zeta/\partial T_0$ (Supplementary Fig. 6).

Data availability

SNOTEL data are available from the Natural Resources Conservation Service, https://www.wcc.nrcs.usda.gov/snow/. NARR output is available from the National Centers for Environmental Information, https://www.ncdc.noaa.gov/data-access/model-data/model-datasets/north-american-regional-reanalysis-narr. The global reanalysis data used here are available from the Global Modeling and Assimilation Office, https://gmao.gsfc.nasa.gov/reanalysis/MERRA-2/.

Code availability

Code for the VIC model is available at: https://vic.readthedocs.io/en/master/. Code used to run the VIC model, analyse model output and observations and generate the plots can be found at https://github.com/amatoevan/snowpack_zeta/.

References

28. Musselman, K. N., Clark, M. P., Liu, C., Ikeda, K. & Rasmussen, R. Slower snowmelt in a warmer world. *Nat. Clim. Change* **7**, 214 (2017).
29. Musselman, K. N., Molotch, N. P. & Margulis, S. A. Snowmelt response to simulated warming across a large elevation gradient, southern Sierra Nevada, California. *Cryosphere* **11**, 2847–2866 (2017).

data and related items of information have not been formally disseminated by NOAA and do not represent any agency determination, view or policy.

Warm Coastal Regions (warmer and small annual cycle, e.g. Pacific Northwest)

$$\frac{\partial \zeta}{\partial T} = -20 \text{ d C}^{-1}$$
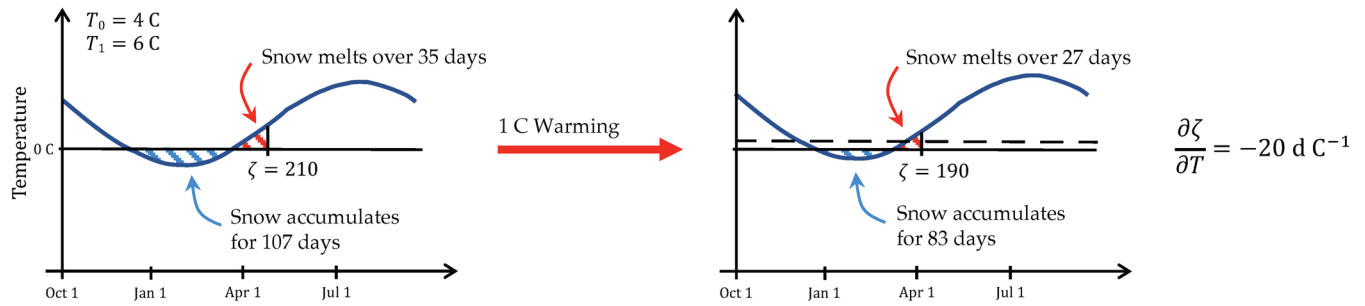
Interior Regions (cooler and large annual cycle, e.g. Colorado Rockies)

$$\frac{\partial \zeta}{\partial T} = -5 \text{ d C}^{-1}$$
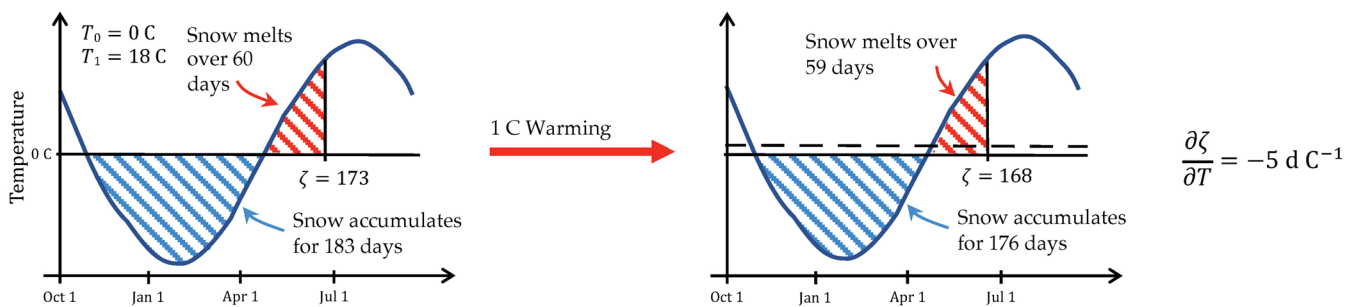
Cold Coastal Regions (cold and small annual cycle, e.g. Coastal Arctic)

$$\frac{\partial \zeta}{\partial T} = -20 \text{ d C}^{-1}$$
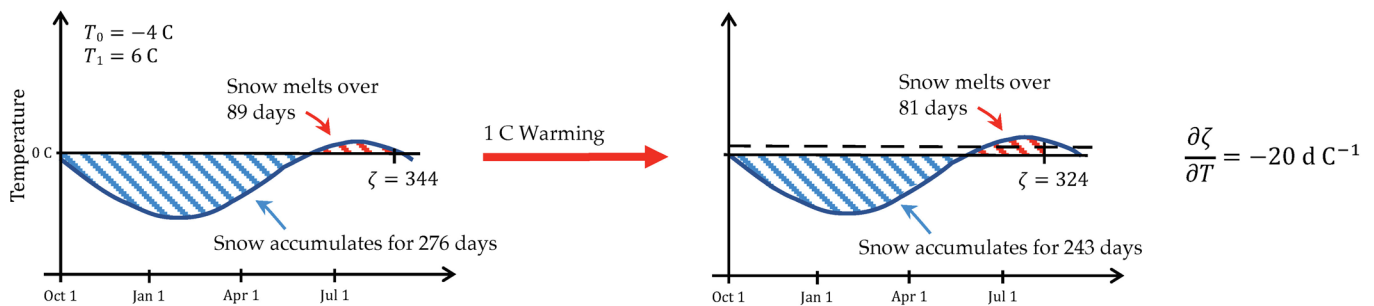
Extended Data Fig. 1 | Schematic illustrating the effect of changes in T_0 and T_1 on $\partial \zeta / \partial T_0$ for three scenarios. Shown are three schematics representing typical annual cycles of temperature (leftmost plots) for a warm coastal region (top), region in the interior of a continent where the annual mean temperature is close to 0 C (middle), and a cold coastal region (bottom). Blue and red hatching indicates periods where $T < 0$ or $T > 0$, respectively. The rightmost plots are the same annual cycles, but for a 1 C increase in annual mean temperature. At far right is the resultant value of $\partial \zeta / \partial T_0$.

Supplementary information

A mechanism for regional variations in snowpack melt under rising temperature

In the format provided by the authors and unedited

A mechanism for regional variations in snowpack melt under rising temperature

Amato Evan,[1*] Ian Eisenman,[1]

[1]Scripps Institution of Oceanography, University of California San Diego,
La Jolla, California, USA

*To whom correspondence should be addressed; E-mail: aevan@ucsd.edu.

This document contains Supplementary Figures 1 to 6
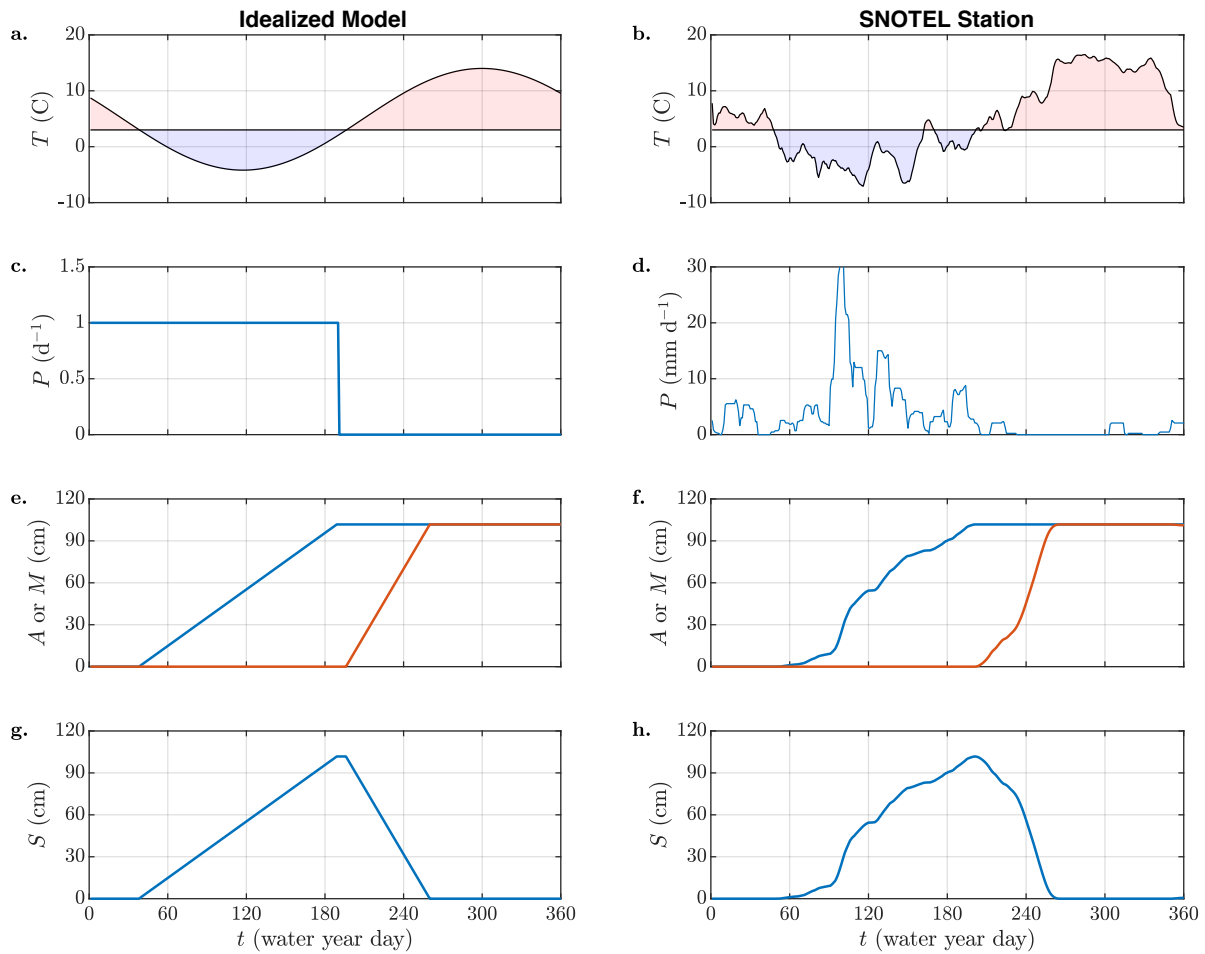
Supplementary Figure 1. Annual time series of temperature (a, b), precipitation (c, d), snowpack accumulation and melt (e, f), and snowpack (g, h) from the idealized model (left column) and SNOTEL observations (right column), corresponding to the Virginia Lakes Ridge SNOTEL station in California for the 2017 water year (as in Fig. 1). The SNOTEL observations have all been smoothed with an 11-day running mean filter. Red and blue shading in 1a and 1b represent time periods when $T > T_m$ and $T < T_m$, respectively.
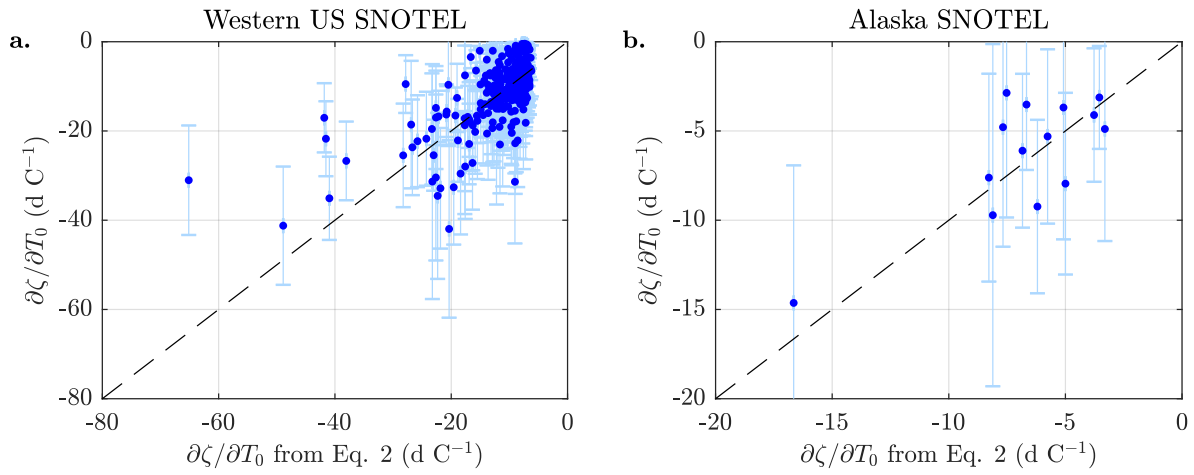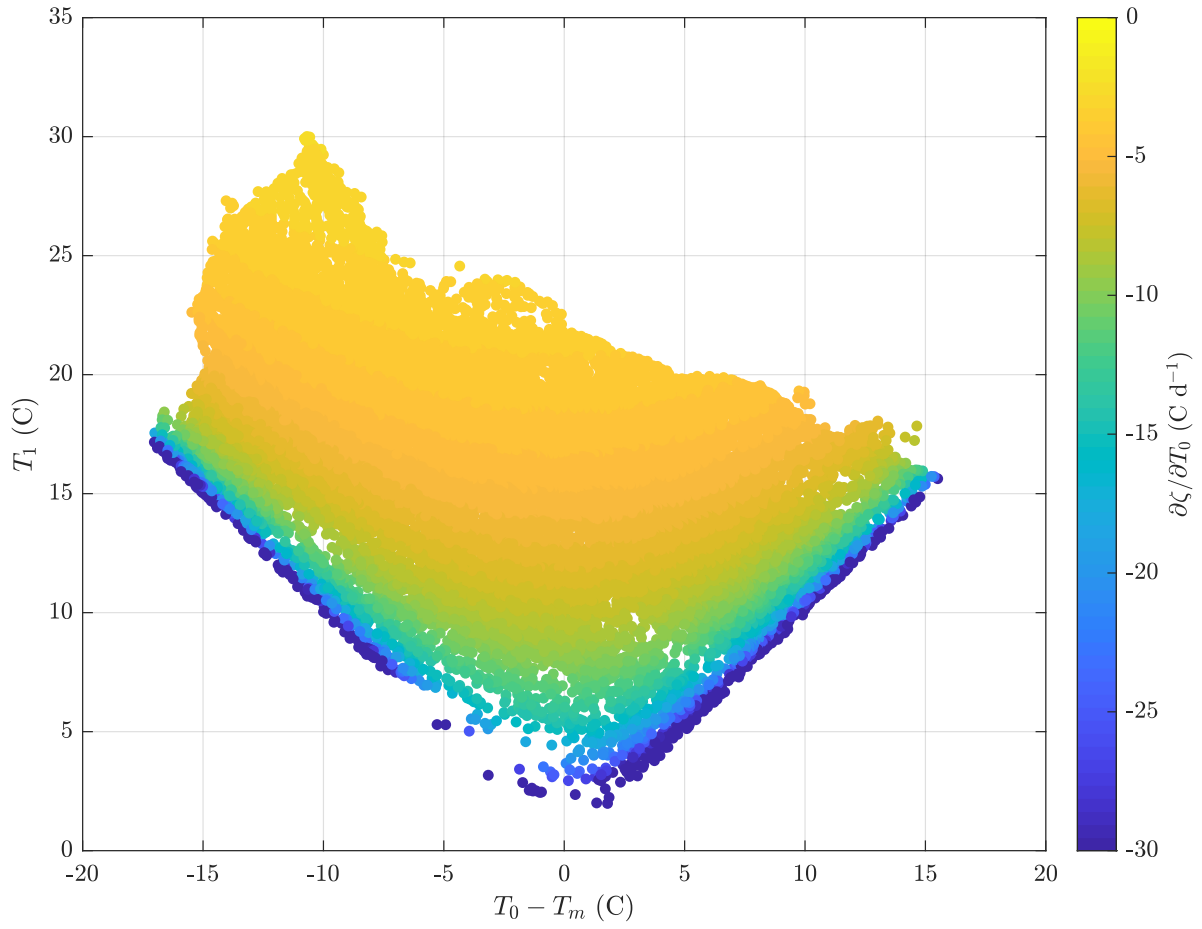
Supplementary Figure 2. As in Fig. 3a in the main text, except that the values of $\partial\zeta/\partial T_0$ are estimated from measurements of S, T, and P made at 363 SNOTEL stations located in the Western US (i.e., south of $50°$N) during the 2001–2018 water years (2a), and 14 SNOTEL stations located in Alaska during the 2008–2018 water years (2b).
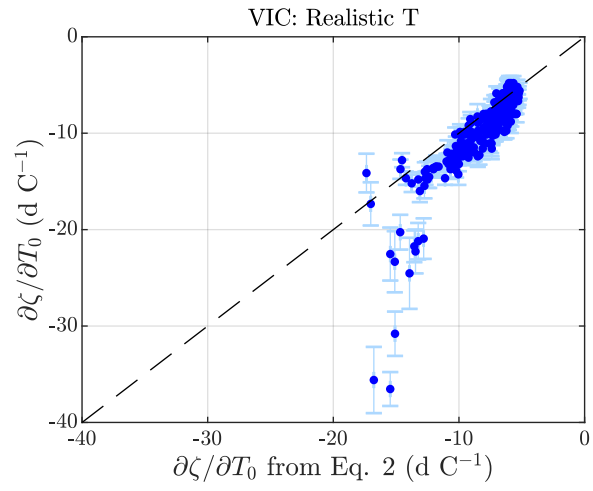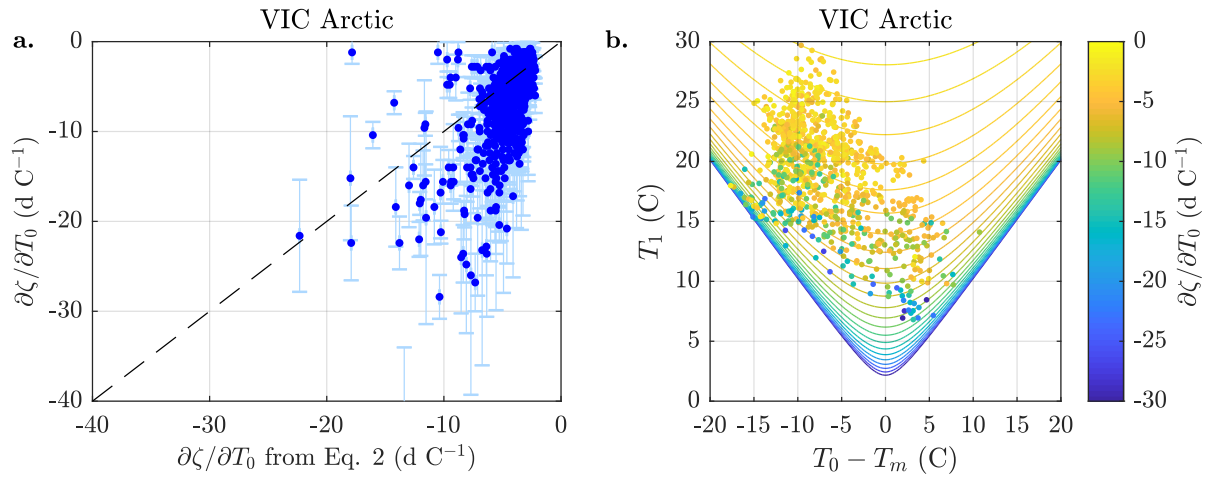
Supplementary Figure 3. As in Fig. 3b except that the daily mean temperature T used to force the VIC model is directly from NARR and thus does not follow a perfect sinusoid (i.e., Eq. 1).

4
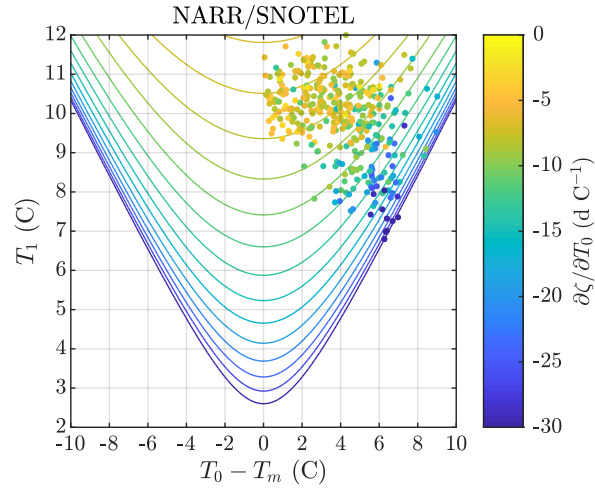
Supplementary Figure 4. Parameter space diagram of $\partial\zeta/\partial T_0$ for SNOTEL sites. Plotted are contours of constant $\partial\zeta/\partial T_0$ as a function of T_1 and $T_0 - T_m$, calculated via Eq. 2 for $R_a/R_m = 0.34$ and $T_m = 0.18$ C. Plotted over these contours (filled circles) are values of $\partial\zeta/\partial T_0$ calculated from the linear regression of SNOTEL measured S and NARR T_0 and P_0.

Supplementary Figure 5. Parameter space diagram of global values of $\partial\zeta/\partial T_0$ (Fig. 4) calculated via Eq. 2 in the main text. Values of T_0 and T_1 are from global reanalysis and calculated over the 1982–2018 water years (see main text). The parameters R_a/R_m and T_m are based on the long-term means of these values, averaged over SNOTEL sites in the Western US (Fig. 2).

Supplementary Figure 6. Comparisons of $\partial\zeta/\partial T_0$ calculated from VIC model output. Description for 6a is the same as that for Fig. 3b, except that the model is forced with output from a global reanalysis (see Materials and Methods) poleward of $60°$N. Description of 6b is the same as that for Supplementary Figure 4, except that the contours are based on mean values of R_a/R_m and T_m calculated from the VIC output, 0.12 and -1.4, respectively, and that the plotted values of $\partial\zeta/\partial T_0$ correspond to those calculated directly from the VIC model output (identical to the vertical axis in 6a).